Spectrally formulated wavelet finite element for wave propagation and impact force identification in connected 1-D waveguides

Mira Mitra, S. Gopalakrishnan *

Department of Aerospace Engineering, Indian Institute of Science, Bangalore 560012, India

Abstract

In this paper, a novel wavelet based spectral finite element is developed for studying elastic wave propagation in 1-D connected waveguides. First the partial differential wave equation is converted to simultaneous ordinary differential equations (ODEs) using Daubechies wavelet approximation in time. These ODEs are then solved using finite element (FE) technique by deriving the exact interpolating function in the transformed domain. Spectral element captures the exact mass distribution and thus the system size required is very much smaller then conventional FE. The localized nature of the compactly supported Daubechies wavelet allows easy imposition of initial-boundary values. This circumvents several disadvantages of the conventional spectral element formulation using Fast Fourier Transforms (FFT) particularly in the study of transient dynamics. The proposed method is used to study longitudinal and flexural wave propagation in rods, beams and frame structures. Numerical experiments are performed to show the advantages over FFT-based spectral element methods. The efficiency of the spectral formulation for impact force identification is also demonstrated.

Keywords: Wavelets; Wave propagation; Finite element; Inverse problem; Force identification; Spectral finite element

1. Introduction

Wavelets have several properties which are encouraging their use for numerical solutions of partial differential equations (PDEs) (Amaratunga et al., 1993, 1994; Qian and Weiss, 1993a,b; Glowinski et al., 1990

* Corresponding author. Tel.: +91 8023603019; fax: +91 8023600134.
E-mail address: krishnan@aero.iisc.ernet.in (S. Gopalakrishnan).

and Joly et al., 1994). Dahmen (2001) has provided a review of wavelet techniques for solution of PDEs. The orthogonal, compactly supported wavelet basis of Daubechies (Daubechis, 1988, 1992) exactly approximates polynomial of increasingly higher order. These wavelet bases can provide accurate and stable representation of differential operations even in region of strong gradients or oscillations. In addition, the orthogonal wavelet bases have the inherent advantage of multi resolution analysis over the traditional methods.

Numerical solution of elastic wave equations requires high accuracy in numerical differentiation and at the same time has larger spatial grids and time steps to make it computationally efficient. Wave propagation problems deal with loadings that have very high frequency content. Finite element formulation for wave propagation problems requires large system size to capture all the higher modes. Hence the element size has to be comparable to wavelengths, which are very small at high frequencies. These problems are usually solved in frequency domain using Fourier methods, which can in principle achieve high accuracy in numerical differentiation. One such method is spectral finite element method (SFEM) developed by Doyle (1999).

In conventional SFEM, first the governing PDE is transformed in frequency domain using FFT in time. For one dimensional (1-D) structures, PDE is reduced to a set of ODEs with constant coefficients, with frequency as a parameter. The resulting ODEs are much easier to solve than the original PDE. These ODEs are then usually solved exactly, which are used as interpolating functions for spectral element formulation. This results in exact mass distribution and dynamic stiffness matrix. Hence, in the absence of any discontinuity, one single element is sufficient to handle an 1-D structure of any length. This substantially reduces the system size and it is many orders smaller compared to conventional FE. First, the exact dynamic stiffness is used to determine the system transfer function (frequency response function). This is then convolved with load. Next, inverse fast Fourier transform (IFFT) is used to get the time history of the response. Such FFT based spectral finite element (FSFE) has been reported in the literature by Doyle (1988) for elementary rod, by Doyle and Farris (1990a,b) for elementary beam, by Gopalakrishnan et al. (1992) for multiply connected one dimensional Timoshenko beam and by Martin et al. (1994) for higher order rod. In the area of composite, FSFE has been developed for Euler–Bernoulli beam by Mahapatra et al. (2000) and for Timoshenko beam by Mahapatra and Gopalakrishnan (2003). FSFE formulation for wave propagation analysis in functionally graded beam is presented Chakraborty and Gopalakrishnan (2003a).

The main drawback of Fourier based spectral approach is that it cannot handle waveguides of short lengths. This is because, short length forces multiple reflections at smaller time scales. Since Fourier transforms are associated with a finite time window (that depends on time sampling rate), shorter lengths of waveguide do not allow the response to die down within the chosen time window, irrespective of the type of damping used in modeling. This forces the response to wrap around, that is the remaining part of the response beyond the chosen time window, will start appearing first. This totally distorts the response. It is in such cases compactly supported wavelets, which have localized basis functions can be efficiently used for waveguides of short lengths. Different wavelet based modeling techniques for simulation of wave propagation have been presented by Hong and Kennett (2002), Joly et al. (1995) and Robertsson et al. (1994).

In the present work an approach similar to SFEM is followed. Daubechies scaling functions are used for approximation in time and this reduces the PDE to ODEs in spatial dimension. These ODEs formed are coupled unlike those in FFT based SFEM (FSFEM). The system of coupled ODEs are decoupled performing an eigenvalue analysis, which decreases the computational cost considerably. The eigen analysis involved is time consuming, but this can be computed and stored as it is not related to the particular problem. The decoupled ODEs are then solved similarly as in SFEM and a wavelet based spectral element (WSFE) is formulated.

In this paper, first, a periodic boundary condition is adapted and for this case the results are expected to be similar to those obtained using FSFEM. Next, an extrapolation technique proposed by Amaratunga and Williams (1995, 1997) and Williams and Amaratunga (1997), is used for adapting wavelet in a finite domain and imposition of initial values. The latter approach is expected to remove the problems associated with

"wrap around" due to the assumed periodicity of solutions in FSFEM and thus may result in smaller time window for the same problem. Further, FSFEM cannot be used for finite length undamped structures. For such cases a semi-infinite element (throw-off element (Doyle, 1999)) is normally used to allow some leakage of response, which in turn amounts to adding artificial damping through the release of trapped energy.

One of the biggest advantages of the spectral approach is in the performance of inverse problems. This is because, in spectral approach, system transfer function which is one of the principle ingredients to perform inverse problem, is obtained as direct byproduct. Force identification is one such inverse problem. Identification of dynamic force from the experimentally measured response at some point is a problem of wide applicability. In many cases like high velocity impact of aircraft by bird hit, gust or tool drop etc., it is difficult to measure the impacting force and the only way is to obtain it inversely from the measured response. The convenience of using SFEM to predict the force history from the measured responses has been demonstrated for mono-material beam, bi-material beam, isotropic and orthotropic plates by Doyle (1984, 1993, 1987a,b) respectively. Similar force identifications using FSFEM were presented by Rizzi and Doyle (1991) for isotropic layered media and by Chakraborty and Gopalakrishnan (2003b, 2004) for inhomogeneous layered media. However, for accurate force identification, complete trace of the measured response is required. Experimentally recorded signals are bound to be truncated. The truncation point proves to be an important factor to determine the accuracy of the reconstructed force in FSFEM. This problem is even more severe in dispersive system, where the wave response will not die down completely within the chosen time window. All these problems occur in FSFEM due to assumed periodicity in both forward and inverse Fourier transforms. This problem is expected to be solved using wavelet transform as no such periodicity is assumed in the formulation of WSFE. In addition, the localized nature of the wavelet basis functions enable easy handling of finite geometries. Hence, as explained in the case of forward problem, the accuracy of the identified force using wavelet based SFEM (WSFEM) is independent of the point of truncation unlike FSFEM.

Wavelet based technique has been used for inverse problems of measuring temperature from sideways heat equation by Reginska (1995), Reginska and Elden (1997) and Elden et al. (2000). Meyer and Daubechies wavelets were used to approximate the time derivative and were compared with Fourier based approximation. In (Doyle, 2002), reconstruction of force is done from experimentally recorded wave response of an impacted plate with hole using wavelet representation of unknown load and FE method. In the present work, truncated FE responses obtained at certain points are used as surrogate experimental responses. These truncated FE responses are given as input to spectral element solver and the force data are reconstructed by performing inverse analysis. Though these truncated responses obtained from FE simulations are used as input, they are free from several complexities associated with experimentally measured response. Vandergheynst et al. (2001), presented a continuous wavelet transform based method for identification of excited modes, moment of rupture and denoising in an impact test.

The organization of the paper is as follows. In Section 2, a brief overview of the orthonormal bases of compactly supported wavelets are presented. In Sections 3–5, the details of wavelet based spectral element formulation are given for isotropic rods and beams. In Section 6, various numerical experiments are presented. First, longitudinal and transverse wave propagations in rods, beams and frames obtained using the formulated element are presented. The results are compared with FSFEM and 2-D FE results for various cases. Next, the element is used for force identification by using surrogate FE responses as input and are compared with those obtained using FSFEM for rods, beams and frame. The paper ends with some important conclusion and scope for further research.

2. Daubechies compactly supported wavelets

In this section, a concise review of orthogonal basis of Daubechies wavelets (Daubechis, 1988, 1992) is provided. Wavelets, $\psi_{j,k}(t)$ form compactly supported orthonormal bases for $\mathbf{L}^2(\mathbf{R})$. The wavelets and

associated scaling functions $\varphi_{j,k}(t)$ are obtained by translation and dilation of single functions $\psi(t)$ and $\varphi(t)$ respectively.

$$\psi_{j,k}(t) = 2^{j/2}\psi(2^j t - k), \quad j,k \in \mathbf{Z} \tag{1}$$

$$\varphi_{j,k}(t) = 2^{j/2}\varphi(2^j t - k), \quad j,k \in \mathbf{Z} \tag{2}$$

The scaling function $\varphi(t)$ is derived from the dilation or scaling equation,

$$\varphi(t) = \sum_k a_k \varphi(2t - k) \tag{3}$$

and the wavelet function $\psi(t)$ is obtained as

$$\psi(t) = \sum_k (-1)^k a_{1-k} \varphi(2t - k) \tag{4}$$

a_k are the filter coefficients and they are fixed for specific wavelet or scaling function basis. For compactly supported wavelets only a finite number of a_k are nonzero.

The filter coefficients a_k are derived by imposing certain constraints on the scaling functions which are as follows. (1). The area under scaling function is normalized to one.

$$\int_{-\infty}^{\infty} \varphi(t)\,\mathrm{d}t = 1 \tag{5}$$

(2) The scaling function $\varphi(t)$ and its translates are orthonormal

$$\int_{-\infty}^{\infty} \varphi(t)\varphi(t+k)\,\mathrm{d}t = \delta_{0,k} \quad k \in \mathbf{Z} \tag{6}$$

and (3) wavelet function $\psi(t)$ has M vanishing moments

$$\int_{-\infty}^{\infty} \psi(t) t^m\,\mathrm{d}t = 0 \quad m = 0, \ldots, M \tag{7}$$

The number of vanishing moments M denotes the order N of the Daubechies wavelet, where $N = 2M$.

The translates of the scaling and wavelet functions on each fixed scale j form orthogonal subspaces,

$$V_j = \{2^{j/2}\varphi(2^j t - k);\ j \in \mathbf{Z}\} \tag{8}$$

$$W_j = \{2^{j/2}\psi(2^j t - k);\ j \in \mathbf{Z}\} \tag{9}$$

such that V_j form a sequence of embedded subspaces

$$\{0\}, \ldots, \subset V_{-1}, \subset V_0, \subset V_1, \ldots, \subset \mathbf{L}^2(\mathbf{R}) \tag{10}$$

and

$$V_{j+1} = V_j \oplus W_j \tag{11}$$

Let $P_j(f)(t)$ be approximation of a function $f(t)$ in $\mathbf{L}^2(\mathbf{R})$ using $\varphi_{j,k}(t)$ as basis, at a certain level (resolution) j, then

$$P_j(f)(t) = \sum_k c_{j,k}\varphi_{j,k}(t), \quad k \in \mathbf{Z} \tag{12}$$

where, $c_{j,k}$ are the approximation coefficients. Let $Q_j(f)(t)$ be the approximation of the function using $\psi_{j,k}(t)$ as basis, at the same level j.

$$Q_j(f)(t) = \sum_k d_{j,k}\psi_{j,k}(t), \quad k \in \mathbf{Z} \tag{13}$$

where, $d_{j,k}$ are the detail coefficients. The approximation $P_{j+1}(f)(t)$ to the next finer level of resolution $j+1$ is given by

$$P_{j+1}(f)(t) = P_j(f)(t) + Q_j(f)(t) \tag{14}$$

This forms the basis of multi resolution analysis associated with wavelet approximation.

3. Reduction of wave equations to ODEs

3.1. Longitudinal wave equation for rods

The governing differential wave equation of an isotropic rod is given as

$$EA\frac{\partial^2 u}{\partial x^2} - \eta A\frac{\partial u}{\partial t} = \rho A\frac{\partial^2 u}{\partial t^2} \tag{15}$$

where, E, A, η and ρ are the Young's modulus, damping ratio, cross sectional area and density respectively. $u(x,t)$ is the axial deformation. Let $u(x,t)$ be discretized at n points in the time window $[0t_f]$. Let $\tau = 0, 1, \ldots, n-1$ be the sampling points, then

$$t = \Delta t\tau \tag{16}$$

where, Δt is the time interval between two sampling points. The function $u(x,t)$ can be approximated by scaling function $\varphi(\tau)$ at an arbitrary scale as

$$u(x,t) = u(x,\tau) = \sum_k u_k(x)\varphi(\tau - k), \quad k \in \mathbf{Z} \tag{17}$$

where, $u_k(x)$ (referred as u_k hereafter) are the approximation coefficient at a certain spatial dimension x. Substituting Eqs. (17) and (16) in Eq. (15) we get,

$$EA\sum_k \frac{\mathrm{d}^2 u_k}{\mathrm{d}x^2}\varphi(\tau - k) - \frac{\eta A}{\Delta t}\sum_k u_k\varphi'(\tau - k) = \frac{\rho A}{\Delta t^2}\sum_k u_k\varphi''(\tau - k) \tag{18}$$

Taking inner product on both sides of Eq. (18) with $\varphi(\tau - j)$, where $j = 0, 1, \ldots, n-1$ we get

$$\begin{aligned} &EA\sum_k \frac{\mathrm{d}^2 u_k}{\mathrm{d}x^2}\int \varphi(\tau - k)\varphi(\tau - j)\mathrm{d}\tau - \frac{\eta A}{\Delta t}\sum_k u_k \int \varphi'(\tau - k)\varphi(\tau - j)\mathrm{d}\tau \\ &\quad = \frac{\rho A}{\Delta t^2}\sum_k u_k \int \varphi''(\tau - k)\varphi(\tau - j)\mathrm{d}\tau \end{aligned} \tag{19}$$

The translates of scaling functions are orthogonal i.e.

$$\int \varphi(\tau - k)\varphi(\tau - j)\mathrm{d}\tau = 0 \quad \text{for } j \neq k \tag{20}$$

Using Eq. (20), Eq. (19) can be written as n simultaneous ODEs

$$EA\frac{\mathrm{d}^2 u_j}{\mathrm{d}x^2} - \frac{\eta A}{\Delta t}\sum_{k=j-N+2}^{j+N-2}\Omega^1_{j-k}u_j = \frac{\rho A}{\Delta t^2}\sum_{k=j-N+2}^{j+N-2}\Omega^2_{j-k}u_k \quad j = 0, 1, \ldots, n-1 \tag{21}$$

$$EA\frac{\mathrm{d}^2u_j}{\mathrm{d}x^2}=\sum_{k=j-N+2}^{j+N-2}\left(\frac{\eta A}{\Delta t}\Omega^1_{j-k}+\frac{\rho A}{\Delta t^2}\Omega^2_{j-k}\right)u_k\quad j=0,1,\ldots,n-1 \tag{22}$$

where, N is the order of the Daubechies wavelet as discussed earlier. Ω^1_{j-k} and Ω^2_{j-k} are the connection coefficients defined as

$$\Omega^1_{j-k}=\int\varphi'(\tau-k)\varphi(\tau-j)\,\mathrm{d}\tau \tag{23}$$

$$\Omega^2_{j-k}=\int\varphi''(\tau-k)\varphi(\tau-j)\,\mathrm{d}\tau \tag{24}$$

For compactly supported wavelets, $\Omega^1_{j-k}, \Omega^2_{j-k}$ are nonzero only in the interval $k=j-N+2$ to $k=j+N-2$. The details for evaluation of connection coefficients for different orders of derivative are given by Beylkin (1992).

The forced boundary condition associated with the governing differential given by Eq. (15) is

$$EA\frac{\partial u}{\partial x}=F \tag{25}$$

where, $F(x,t)$ is the axial force applied. $F(x,t)$ can be approximated similarly as $u(x,t)$ in Eq. (17)

$$F(x,t)=F(x,\tau)=\sum_k F_k(x)\varphi(\tau-k),\quad k\in\mathbf{Z} \tag{26}$$

Substituting Eqs. (17) and (26) in Eq. (25) and taking the inner product with $\varphi(\tau-j)$ we get,

$$EA\frac{\mathrm{d}u_j}{\mathrm{d}x}=F_j\quad j=0,1,\ldots,n-1 \tag{27}$$

While dealing with finite length data sequence, problems arise at the boundaries. It can be observed from the ODEs given by Eq. (22) that certain coefficients u_j near the vicinity of the boundaries ($j=0$ and $j=n-1$) lie outside the time window $[0t_f]$ defined by $j=0,1,\ldots,n-1$. Several approaches like capacitance matrix methods (Qian and Weiss, 1993a,b), penalty function methods for treating boundaries are reported in the literature. In this paper, first a circular convolution method is adopted assuming periodicity of the solution. The solution obtained by this method is exactly similar to those obtained using FSFEM. Next, a wavelet based extrapolation scheme proposed by Amaratunga and Williams (1995, 1997) and Williams and Amaratunga (1997), is implemented for solution of boundary value problems. This approach allows treatment of finite length data and uses polynomial to extrapolate wavelet coefficients at boundaries either from interior coefficients or boundary values. The method is particularly suitable for approximation in time for the ease to impose initial values. The details of the formulation in given in Section 4.

After treating the boundaries for analysis of finite system, the simultaneous ODEs and associated boundary conditions (Eqs. (22) and (27)) are solved using spectral element methods. The formulation of spectral element is described in detail in Section 5. Prior to these, the flexural wave equation for beams are reduced to ODEs following similar approach as in rod. This is discussed in the next subsection.

3.2. Flexural wave equation for beams

The flexural wave equation for beam has a fourth order derivative in space and is given as

$$EI\frac{\partial^4 w}{\partial x^4}+\eta A\frac{\partial w}{\partial t}+\rho A\frac{\partial^2 w}{\partial t^2}=0 \tag{28}$$

where, $w(x,t)$ is the transverse displacement and I is the moment of inertia of the cross section. The main difference between longitudinal and flexural waves is that the later is dispersive, in other words the wave speeds vary with frequencies.

The transverse displacement $w(x,t)$ is approximated as

$$w(x,t) = w(x,\tau) = \sum_k w_k(x)\varphi(\tau - k), \quad k \in \mathbf{Z} \tag{29}$$

where, $w_k(x)$ (referred as w_k hereafter) are the approximation coefficients. Substituting Eq. (29) in Eq. (28) and following similar steps of Eqs. (16), (19) and (20), we get the reduced ODEs as

$$EI\frac{\mathrm{d}^4 w_j}{\mathrm{d}x^4} + \frac{\eta A}{\Delta t}\sum_{k=j-N+2}^{j+N-2} \Omega^1_{j-k} w_j + \frac{\rho A}{\Delta t^2}\sum_{k=j-N+2}^{j+N-2} \Omega^2_{j-k} w_k = 0 \quad j = 0,1,\ldots,n-1 \tag{30}$$

$$EI\frac{\mathrm{d}^4 w_j}{\mathrm{d}x^4} + \sum_{k=j-N+2}^{j+N-2}\left(\frac{\eta A}{\Delta t}\Omega^1_{j-k} + \frac{\rho A}{\Delta t^2}\Omega^2_{j-k}\right) w_k = 0 \quad j = 0,1,\ldots,n-1 \tag{31}$$

The forced boundary conditions associated with the governing equation (28) are

$$EI\frac{\partial^2 w}{\partial x^2} = M \tag{32}$$

$$EI\frac{\partial^3 w}{\partial x^3} = -V \tag{33}$$

where M and V are the applied moment and transverse force respectively. Similar to Eq. (26), $M(x,t)$ and $V(x,t)$ are written as

$$M(x,t) = M(x,\tau) = \sum_k M_k(x)\varphi(\tau - k), \quad k \in \mathbf{Z} \tag{34}$$

$$V(x,t) = V(x,\tau) = \sum_k V_k(x)\varphi(\tau - k), \quad k \in \mathbf{Z} \tag{35}$$

Substituting Eqs. (34) and (35) in Eqs. (32) and (33) respectively we get the following ODEs

$$EI\frac{\mathrm{d}^2 w_j}{\mathrm{d}x^2} = M_j \quad j = 0,1,\ldots,n-1 \tag{36}$$

$$EI\frac{\mathrm{d}^3 w_j}{\mathrm{d}x^3} = -V_j \quad j = 0,1,\ldots,n-1 \tag{37}$$

Spectral element for beam is formulated using the ODEs given by Eqs. (31), (36) and (37). In the following sections the formulation and numerical experiments are given for both rod and beam and finally for 2-D frames.

4. Boundary value problem

In this section, the treatment of boundaries for finite domain analysis is given. From Eq. (22) of previous section, we get n coupled ODEs, which are to be solved for u_j using method described later. For numerical implementation, we can deal with only finite sequence. In other words, $u(x,t)$ and hence u_j are only known in the interval $[0, t_f]$ and $j = 0$ to $j = n-1$. In Eq. (22), the ODEs corresponding to $j = 0$ to $j = N-2$, contain

coefficients u_j that lie outside the $[0, t_f]$. Similarly, on the other boundary, for $j = (n-1)-N+2$ to $j = (n-1)$ same problem exists. In the remaining part of this section, the details of two approaches adopted to solve this boundary value problem are provided.

4.1. Periodic boundary condition

In this approach, the function $u(x,t)$ is assumed to be periodic in time, with time period t_f. Thus the unknown coefficients on LHS are taken as

$$\begin{aligned} u_{-1} &= u_{n-1} \\ u_{-2} &= u_{n-2} \\ &\vdots \\ u_{-N+2} &= u_{n-N+2} \end{aligned} \tag{38}$$

Similarly the unknown coefficients on RHS i.e. $u_n, u_{n+1}, \ldots, u_{n+N-2}$ are equal to $u_0, u_1, \ldots, u_{N-2}$ respectively. With the above assumption, the coupled ODEs given by Eq. (22) can be written in matrix form as

$$\left\{\frac{\mathrm{d}^2 u_j}{\mathrm{d}x^2}\right\} = \left(\frac{\eta A}{EA}\Lambda^1 + \frac{\rho A}{EA}\Lambda^2\right)\{u_j\} \tag{39}$$

where, Λ^1 and Λ^2 are $n \times n$ circulant connection coefficient matrices and have the form

$$\Lambda^1 = \frac{1}{\Delta t}\begin{bmatrix} \Omega^1_0 & \Omega^1_{-1} & \ldots & \Omega^1_{-N+2} & \ldots & \Omega^1_{N-2} & \ldots & \Omega^1_1 \\ \Omega^1_1 & \Omega^1_0 & \ldots & \Omega^1_{-N+3} & \ldots & 0 & \ldots & \Omega^1_2 \\ \vdots & \vdots & \ldots & \vdots & \ldots & \vdots & \ldots & \vdots \\ \Omega^1_{-1} & \Omega^1_{-2} & \ldots & 0 & \ldots & \Omega^1_{N-3} & \ldots & \Omega^1_0 \end{bmatrix} \tag{40}$$

Λ^2 for second order derivative has a similar form. For a circulant matrix Λ^1 (Davis, 1963), the eigenvalues λ_α are

$$\lambda_\alpha = \sum_{k=-N+2}^{N-2} \Omega^1_k \mathrm{e}^{-2\pi \mathrm{i}\alpha k/n} \quad \alpha = 0, 1, \ldots, n-1 \tag{41}$$

and the corresponding orthonormal eigenvector v_α, $\alpha = 0, 1, \ldots, n-1$ are

$$(v_\alpha)_k = \frac{1}{\sqrt{n}}\mathrm{e}^{-2\pi \mathrm{i}\alpha k/n}, \quad k = 0, 1, \ldots, n-1 \tag{42}$$

As discussed earlier, the spectral element formulation in the later part of the paper, involves eigenvalue analysis. This is done to diagonalize the matrix in Eq. (39) and decouple the ODEs. For periodic boundary condition, these eigenvalues are known analytically and hence decreases the computational cost. However, the solutions obtained are same as those obtained using FSFEM and possess several problems such as wrap around due to assumed periodicity of the solution.

4.2. Non-periodic boundary condition

In this section boundaries are treated using wavelet extrapolation method for Daubechies compactly supported wavelets. The detail of the formulation is given in (Amaratunga and Williams, 1995, 1997 and Williams and Amaratunga, 1997), here a brief outline is presented for completeness.

In this method a polynomial of order $p-1$, ($p = N/2$) is assumed to extrapolate the values at the boundaries. Since, in this work the wavelets are used in time, the unknown coefficients on the LHS (i.e. $u_{-1}, u_{-2}, \ldots, u_{-N+2}$) are extrapolated from the initial values. The coefficients $u_n, u_{n+1}, \ldots, u_{n+N-2}$ on RHS are extrapolated from the known coefficients $u_{(n-1)-p+1}, u_{(n-1)-p+2}, \ldots, u_{n-1}$.

Assuming polynomial representation of order $p-1$ for u in the vicinity of $t = 0$ and using Eq. (17)

$$u(x,\tau) = \sum_k u_k(x)\varphi(\tau - k) = \sum_{l=0}^{p-1} c_l \tau^l \tag{43}$$

where c_l are constant coefficients. Taking inner product on both sides of Eq. (43) and using Eq. (20), we get

$$u_j = \sum_{l=0}^{p-1} c_l \mu_j^l \quad j = -1, -2, \ldots, -N+2 \tag{44}$$

where, μ_j^l are the moments of the scaling function defined as

$$\mu_j^l = \int_{-\infty}^{\infty} \tau^l \varphi(\tau - j)\mathrm{d}\tau \tag{45}$$

and are derived by solving a recursive equation (Latto et al., 1991). Solution of Eq. (43) to obtain c_l requires $p-1$ initial values of $u(x,\tau)$ at $\tau = 0, 1, \ldots, p-1$ and these may be obtained using schemes like finite difference. Next, the values of c_l obtained in terms of the initial values are substituted back into Eq. (44). Thus the unknown coefficients u_j, $j = -1, -2, \ldots, -N+2$ are obtained as

$$\begin{bmatrix} u_{-1} \\ u_{-2} \\ \vdots \\ u_{-N+2} \end{bmatrix} = \begin{bmatrix} \mu_{-1}^0 & \mu_{-1}^1 & \cdots & \mu_{-1}^{p-1} \\ \mu_{-2}^0 & \mu_{-2}^1 & \cdots & \mu_{-2}^{p-1} \\ \vdots & \vdots & \cdots & \vdots \\ \mu_{-N+2}^0 & \mu_{-N+2}^1 & \cdots & \mu_{-N+2}^{p-1} \end{bmatrix} \begin{bmatrix} c_0 \\ c_1 \\ \vdots \\ c_{p-1} \end{bmatrix} \tag{46}$$

The unknown coefficients at the RHS boundary are evaluated assuming the same polynomial representation and

$$u_j = \sum_{l=0}^{p-1} c_l \mu_{j-n}^l \quad j = (n-1) - p + 1, (n-1) - p + 2, \ldots, n-1 \tag{47}$$

Eq. (47) can be written in matrix form as

$$\begin{bmatrix} \mu_{-p}^0 & \mu_{-p}^1 & \cdots & \mu_{-p}^{p-1} \\ \mu_{-p+1}^0 & \mu_{-p+1}^1 & \cdots & \mu_{-p+1}^{p-1} \\ \vdots & \vdots & \cdots & \vdots \\ \mu_{-1}^0 & \mu_{-1}^1 & \cdots & \mu_{-1}^{p-1} \end{bmatrix} \begin{bmatrix} c_0 \\ c_1 \\ \vdots \\ c_{p-1} \end{bmatrix} = \begin{bmatrix} u_{(n-1)-p+1} \\ u_{(n-1)-p+2} \\ \vdots \\ u_{(n-1)} \end{bmatrix} \tag{48}$$

The c_l obtained are then substituted into Eq. (47) for $j = n, n+1, \ldots, n+N-2$ to derive $u_{(n-1)-p+1}$, $u_{(n-1)-p+2}, \ldots, u_{n-1}$ as

$$\begin{bmatrix} u_n \\ u_{n+1} \\ \vdots \\ u_{n-1+N-2} \end{bmatrix} = \begin{bmatrix} \mu_0^0 & \mu_0^1 & \dots & \mu_0^{p-1} \\ \mu_1^0 & \mu_1^1 & \dots & \mu_1^{p-1} \\ \vdots & \vdots & \dots & \vdots \\ \mu_{-N+2}^0 & \mu_{-N+2}^1 & \dots & \mu_{-N+2}^{p-1} \end{bmatrix} \begin{bmatrix} c_0 \\ c_1 \\ \vdots \\ c_{p-1} \end{bmatrix} \tag{49}$$

Finally these coefficients are substituted in Eq. (22) and the system of ODEs can be written in a matrix form similar to Eq. (39) as,

$$\left\{\frac{\mathrm{d}^2 u_j}{\mathrm{d}x^2}\right\} = \left(\frac{\eta A}{EA}\Gamma^1 + \frac{\rho A}{EA}\Gamma^2\right)\{u_j\} \tag{50}$$

It should be noted that though all the formulations are done with reference to the governing differential equation for rod, the connection coefficient matrices Λ^1, Λ^2 and Γ^1, Γ^1 are independent of problem and depend only on the order of wavelet i.e. N. Hence the system of ODEs for beam (Eq. (31)) can be written in matrix form as

$$\frac{\mathrm{d}^4 w_j}{\mathrm{d}x^4} + \left(\frac{\eta A}{EI}\Lambda^1 + \frac{\rho A}{EI}\Lambda^2\right) w_j = 0 \quad j = 0, 1, \dots, n-1 \tag{51}$$

or,

$$\frac{\mathrm{d}^4 w_j}{\mathrm{d}x^4} + \left(\frac{\eta A}{EI}\Gamma^1 + \frac{\rho A}{EI}\Gamma^2\right) w_j = 0 \quad j = 0, 1, \dots, n-1 \tag{52}$$

It can be seen from the above derivations that the wavelet coefficients of first and second derivatives can be obtained as

$$\{\dot{u}_j\} = \Lambda^1\{u_j\} \tag{53}$$

$$\{\ddot{u}_j\} = \Lambda^2\{u_j\} \tag{54}$$

The second derivative can also be written as

$$\{\ddot{u}_j\} = \Lambda^1\{\dot{u}_j\} \tag{55}$$

Substituting Eq. (53) in Eq. (55) we get

$$\{\ddot{u}_j\} = [\Lambda^1]^2\{u_j\} \tag{56}$$

Thus though the second order connection coefficient matrices Λ^2 and Γ^2 can be evaluated independently (Beylkin, 1992), they can also written as

$$\Lambda^2 = [\Lambda^1]^2 \tag{57}$$

and

$$\Gamma^2 = [\Gamma^1]^2 \tag{58}$$

5. Spectral element formulation

From the previous sections, we get a system of coupled ODEs for both rods and beams in a transformed wavelet domain. These equations are required to be solved for u_j, w_j and the actual solutions $u(x,t)$, $w(x,t)$ are obtained using inverse wavelet transform. For finite length data, the wavelet transform and its inverse

can be obtained using a transformation matrix. The transformation of a data sequence of length n, involves a $n \times n$ transformation matrix (Williams and Amaratunga, 1994) that can be derived from equation similar to Eq. (17), for $\tau = 0, 1, \ldots, n-1$. These equations also involve coefficients that lies outside the finite interval and the matrix is obtained either by circular convolution or wavelet extrapolation. In Eq. (17), $\varphi(\tau-k)$ is nonzero for $0 < (\tau-k) < N-2$ for Daubechies wavelet.

As discussed earlier in FSFEM (Doyle, 1999), the governing PDEs are reduced to a set of ODEs by FFT. These ODEs are solved exactly, which are then used as interpolation function for SFE formulation. The exact interpolating functions capture the exact mass distribution of the structure. In this paper, a similar approach is adopted for solving the ODEs obtained through wavelet transform. In this section, elements are formulated for rod and beam, which are combined together as in FE to obtain the frame spectral element.

In WSFEM, the reduced ODEs are coupled unlike those in FSFEM. However, the system of equation can be decoupled by diagonalizing the connection coefficient matrix. This can be done by eigenvalue analysis of the matrix as

$$\Gamma^1 = \Phi \Pi \Phi^{-1} \tag{59}$$

where, Φ is the eigenvector matrix of Γ^1 and Π is the diagonal matrix containing corresponding eigenvalues λ_j. Similar expression holds for Λ^1 where Φ and Π are known analytically (Eqs. (42) and (41)). From Eq. (58), Γ^2 can be written as

$$\Gamma^2 = \Phi \Pi^2 \Phi^{-1} \tag{60}$$

where, Π^2 is a diagonal matrix with diagonal terms λ_j^2. This eigenvalue analysis is costly but can be done once and stored as it is completely independent of the problem. This makes the computational time comparable to FSFEM.

5.1. Spectral element for rod

Fig. 1(a) shows the spectral rod element with two nodes and one longitudinal degree of freedom (dof) $\hat{u}_j$ and nodal axial load $\widehat{F}_j$ at each node. The formulation of 2×2 elemental dynamic stiffness matrix is explained as follows. The ODEs obtained by decoupling the Eq. (50) (and similarly Eq. (39)) can be written as

$$\frac{\mathrm{d}^2 \hat{u}_j}{\mathrm{d}x^2} = \left(\frac{\eta A}{EA} \lambda_j + \frac{\rho A}{EA} \lambda_j^2 \right) \hat{u}_j \quad j = 0, 1, \ldots, n-1 \tag{61}$$

where

$$\hat{u}_j = \Phi^{-1} u_j \tag{62}$$

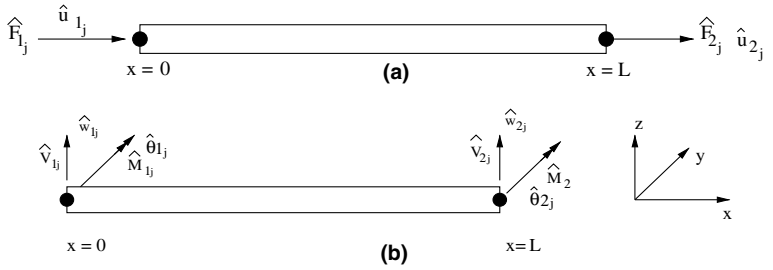

Fig. 1. (a) Rod element and (b) beam element with nodal forces and displacements.

Similarly, the force boundary condition given by Eq. (27) can be written as

$$\frac{\mathrm{d}\hat{u}_j}{\mathrm{d}x} = \widehat{F}_j \quad j = 0, 1, \ldots, n-1 \tag{63}$$

where,

$$\widehat{F}_j = \Phi^{-1} F_j \tag{64}$$

The exact interpolating function obtained by solving Eq. (61) are

$$\hat{u}_j(x) = A_j \mathrm{e}^{-\beta_j x} + B_j \mathrm{e}^{-\beta_j (L-x)} \quad \text{where } \beta_j = \left(\frac{\eta A}{EA} \lambda_j + \frac{\rho A}{EA} \lambda_j^2 \right)^{\frac{1}{2}} \tag{65}$$

The constants $\{a_j\} = \{A_j, B_j\}^{\mathrm{T}}$ are obtained from the boundary conditions at the two nodes (see Fig. 1(a)) i.e. $\hat{u}_j(0) = \hat{u}_{1_j}$ and $\hat{u}_j(L) = \hat{u}_{2_j}$. This can be written as

$$\{\hat{u}_j\} = [B]\{a_j\} \quad \text{where } \{\hat{u}_j\} = \{\hat{u}_{1_j}, \hat{u}_{2_j}\}^{\mathrm{T}} \tag{66}$$

where the matrix $[B]$ is

$$[B] = \begin{bmatrix} 1 & -\mathrm{e}^{-\beta_j L} \\ -\mathrm{e}^{-\beta_j L} & 1 \end{bmatrix} \tag{67}$$

Force boundary condition at the nodes, (see Fig. 1(a)) i.e. $\widehat{F}_j(0) = -\widehat{F}_{1_j}$ and $\widehat{F}_j(L) = \widehat{F}_{2_j}$ are used in Eq. (64) and we get

$$\{\widehat{F}_j\} = [C]\{a_j\} \quad \text{where } \{\widehat{F}_j\} = \{\widehat{F}_{1_j}, \widehat{F}_{2_j}\}^{\mathrm{T}} \tag{68}$$

where the matrix $[C]$ is

$$[C] = EA\beta_j \begin{bmatrix} 1 & -\mathrm{e}^{-\beta_j L} \\ -\mathrm{e}^{-\beta_j L} & 1 \end{bmatrix} \tag{69}$$

From Eqs. (66) and (68) we can obtain a relation between transformed nodal forces and displacements similar to conventional FE

$$\{\widehat{F}_j\} = [C][B]^{-1}\{\hat{u}_j\} = [\widehat{K}]\{\hat{u}_j\} \tag{70}$$

where $[\widehat{K}]$ is the dynamic stiffness matrix. After the constants $\{a_j\}$ are known from the above equation, they can substituted back to Eq. (65) to obtain $\hat{u}_j$ at any given x.

5.2. Spectral element for beam

Fig. 1(b) shows the beam spectral finite element with node and two dofs $\hat{w}_j$ and $\partial\hat{w}_j/\partial x$ at each nodes. The nodal transverse forces and moments are $\widehat{V}_j$ and $\widehat{M}_j$ respectively. Spectral element formulation for beam is very similar to that for rod. The only difference is that the governing differential equation for beam involves fourth order derivative in space and this makes the waves dispersive in nature. The equations obtained by decoupling the system in Eq. (52) (and Eq. (51)) are

$$\frac{\mathrm{d}^4\hat{w}_j}{\mathrm{d}x^4} + \left(\frac{\eta A}{EI} \lambda_j + \frac{\rho A}{EI} \lambda_j^2 \right) \hat{w}_j = 0 \quad j = 0, 1, \ldots, n-1 \tag{71}$$

where,

$$\hat{w}_j = \Phi^{-1} w_j \tag{72}$$

The forced boundary conditions given in Eqs. (36) and (37) are similarly transformed as

$$EI\frac{\mathrm{d}^2\hat{w}_j}{\mathrm{d}x^2} = \widehat{M}_j \quad j = 0, 1, \ldots, n-1 \tag{73}$$

$$EI\frac{\mathrm{d}^3\hat{w}_j}{\mathrm{d}x^3} = -\widehat{V}_j \quad j = 0, 1, \ldots, n-1 \tag{74}$$

The solutions of Eq. (71) are

$$\hat{w}_j(x) = A_j\mathrm{e}^{-\imath\gamma_j x} + B_j\mathrm{e}^{-\imath\gamma_j(L-x)} + C_j\mathrm{e}^{-\gamma_j x} + D_j\mathrm{e}^{-\gamma_j(L-x)} \tag{75}$$

where

$$\gamma_j = \left(\frac{\eta A}{EA}\lambda_j + \frac{\rho A}{EA}\lambda_j^2\right)^{\frac{1}{4}}$$

Next, steps similar to Eq. (66) and (68) are followed to obtain Eq. (70). However, for beam $\{a_j\} = \{A_j, B_j, C_j, D_j\}^{\mathrm{T}}$, the nodal displacements $\{\hat{w}_j\} = \{\hat{w}_{1_j}, \partial\hat{w}_{1_j}/\partial x, \hat{u}_{2_j}, \partial\hat{w}_{2_j}/\partial x\}^{\mathrm{T}}$ and $\{\widehat{F}_j\} = \{\widehat{V}_{1_j}, , \widehat{M}_{1_j}\widehat{V}_{2_j}, \widehat{M}_{2_j}\}^{\mathrm{T}}$ (see Fig. 1(b)) and the $[\widehat{K}]$ is 4×4. The explicit form of $[B]$ and $[C]$ for beam are given as

$$[B] = \begin{bmatrix} 1 & \mathrm{e}^{-\imath\gamma_j L} & 1 & \mathrm{e}^{-\gamma_j L} \\ -\imath\gamma_j & \imath\gamma_j\mathrm{e}^{-\imath\gamma_j L} & -\gamma_j & \gamma_j\mathrm{e}^{-\gamma_j L} \\ \mathrm{e}^{-\imath\gamma_j L} & 1 & \mathrm{e}^{-\gamma_j L} & 1 \\ -\imath\gamma_j\mathrm{e}^{-\imath\gamma_j L} & \imath\gamma_j & -\gamma_j\mathrm{e}^{-\gamma_j L} & \gamma_j \end{bmatrix} \tag{76}$$

$$[C] = (EI\gamma_j^2)\begin{bmatrix} \imath\gamma_j & \imath\gamma_j\mathrm{e}^{-\imath\gamma_j L} & -\gamma_j & -\gamma_j\mathrm{e}^{-\gamma_j L} \\ 1 & \mathrm{e}^{-\imath\gamma_j L} & -1 & -\mathrm{e}^{-\gamma_j L} \\ -\imath\gamma_j\mathrm{e}^{-\imath\gamma_j L} & -\imath\gamma_j & \gamma_j\mathrm{e}^{-\gamma_j L} & \gamma_j \\ -\mathrm{e}^{-\imath\gamma_j L} & -1 & \mathrm{e}^{-\gamma_j L} & 1 \end{bmatrix} \tag{77}$$

5.3. Force identification

The basic idea of SFEM is to obtain a system transfer function that relates the input to the output. From WSFE formulation given in previous sections, the transform of the load $\widehat{F}_j$ and displacements $\widehat{u}_j$ can be related through transfer function $\widehat{G}_j(x)$ as

$$\widehat{u}_j(x) = \widehat{G}_j(x)\widehat{F}_j(x) \tag{78}$$

Other parameters like stress, velocity, strain etc are related to load and displacements and can be used as input or output with required modification in $\widehat{G}_j(x)$. The inverse problem of calculating the input force $\widehat{F}_j$ can be done as

$$\widehat{F}_j(x) = \hat{u}_j(x)/\widehat{G}_j(x) \tag{79}$$

The system transfer function $\widehat{G}_j(x)$ is obtained as follows. After the global $[\widehat{K}]$ is formed, the structure is solved for unit impulse at the desired location. This will directly give $\widehat{G}_j(x)$. The measured response $u(x,t)$ in the time domain is then transformed to the wavelet domain to get $\hat{u}_j(x)$. Then Eq. (79) is used to obtain the force history in wavelet domain, which is then transformed by inverse wavelet transform to obtain required force history.

6. Numerical experiments

Here, first the formulated wavelet spectral element is compared with 2-D FE. It is later used to study axial and flexural wave propagations in 2-D frame. As pointed out earlier, FSFEM has several disadvantages due to the required assumption of periodicity. Such problems can be circumvented using wavelets. Several numerical experiments are presented in this section which support the above statement.

Spectral element is particularly suitable for force identification. The applied force is reconstructed from experimentally measured responses. However, here FE results are used as surrogate experimental data. As discussed in Section 1, the point of truncation of the responses, is a decisive factor for the accuracy of the identified force in conventional SFEM. The numerical examples provided show that such problems are completely eliminated by use of wavelet transform here.

6.1. Wave propagation analysis

First, wave propagation analysis is done for an aluminum rod with Young's modulus $E = 70$ GPa and density $\rho = 2.7 \times 10^3$ kg/m^3. The rod is fixed at one end and an axial impulse load is applied at the free end. The load shown in Fig. 2 has an unit amplitude and duration of 50 μs with a frequency content of 44 kHz. The length, width and depth of the rod are $L = 20$ in., $b = 1$ in. and $h = 0.01$ in. respectively.

Fig. 3(a) shows the tip longitudinal velocity in undamped ($\eta = 0$) rod due impact load applied at tip. The result obtained using a single formulated spectral element is compared with FE results. The FE results are obtained using 400 3-noded plane stress triangular elements and Newmarks time integration with time step 1 μs. For the all the FE results presented hereafter, the above Newmarks scheme is used for time integration unless otherwise mentioned. The wavelet basis function used in this example and elsewhere has an order of $N = 8$ and the sampling rate $\Delta t = 1$ μs unless otherwise mentioned. Thus for a time window $T_w = 512$ μs, the number of sampling points is $n = 512$ and the system size is 512×512. It can be seen that the FE results match well with those obtained using formulated WSFE. FSFEM cannot be used for wave propagation analysis of such undamped finite length structures, where multiple reflections from the boundaries and wrap around completely distort the solution.

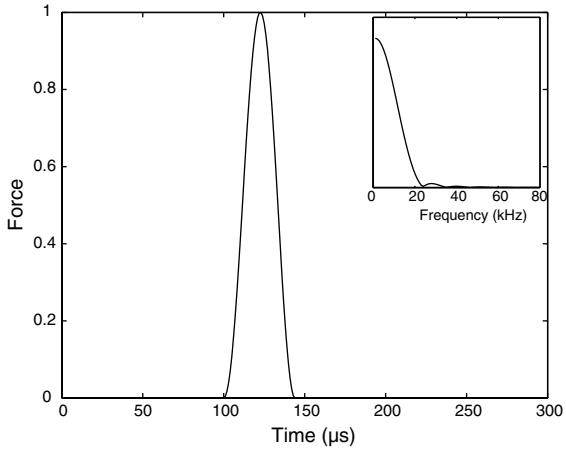

Fig. 2. Impact load and Fourier transform of the load (inset).

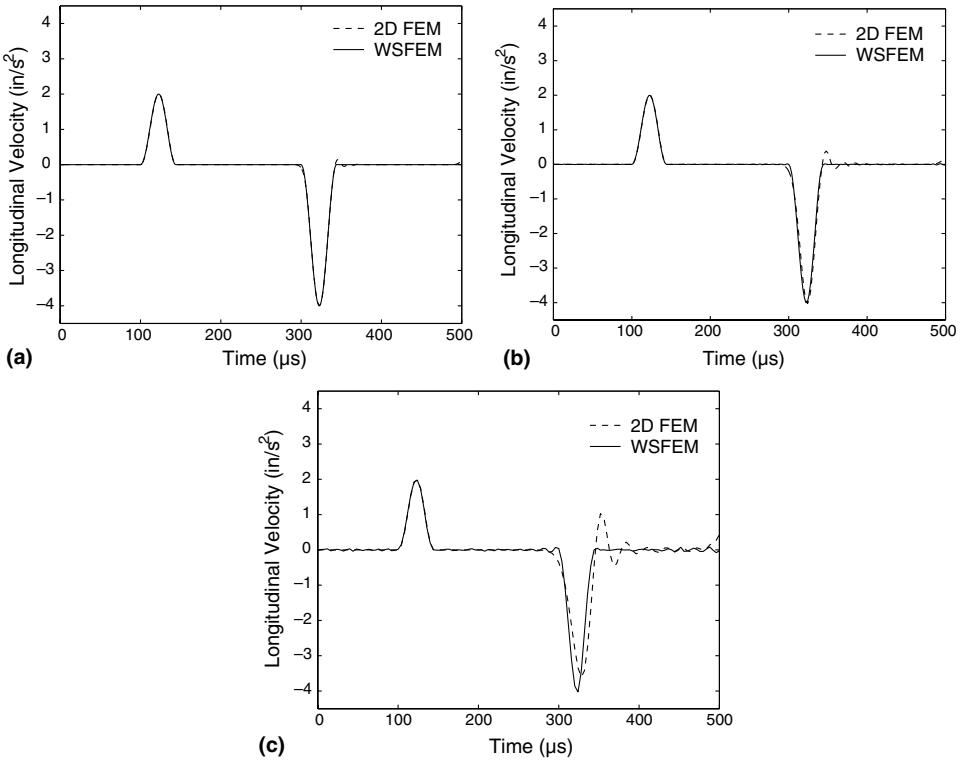

Fig. 3. Longitudinal tip velocity in rod due to tip impact load simulated with time interval (a) $\Delta t = 1$ μs, (b) $\Delta t = 2$ μs and (c) $\Delta t = 4$ μs.

In Fig. 3(b) and (c), the FE results obtained using the above mesh (400 3-noded plane stress triangular elements) but with time steps of 2 μs and 4 μs for Newmarks time integration are presented. These are compared with corresponding WSFE results obtained with $\Delta t = 2$ μs and 4 μs respectively. The time window T_w is kept fixed at 512 μs. It can be seen from Fig. 3(a)–(c) that as the time step is increased, the FE method with Newmarks time integration scheme gradually shows distortions. However, WSFE is free from such distortions even at $\Delta t = 4$ μs.

In Table 1, the CPU time taken by FE and WSFE methods for the above numerical examples are presented for $\Delta t = 1$ μs, 2 μs and 4 μs. The numerical experiments are performed on an IBM IntelliStation

Table 1
CPU time taken by FE with Newmarks time integration and WSFE methods for simulation of longitudinal tip velocity in rod shown in Fig. 3

Time interval Δt (μs)	CPU time (s)	
	2-D FE	Present (WSFE)
1	54.00	18.00
2	27.00	2.00
4	15.00	1.00

workstation (with Intel Pentium 4 processor). It can be seen that the CPU time taken by the present WSFE method is much less than that taken by FE method. In addition, it can be seen from Fig. 3(c) that for $\Delta t = 4$ μs, WSFE solution is much more accurate than the corresponding FE solution. This leads to further computational savings in WSFEM compared over FE analysis with Newmarks time integration.

Wave propagation analysis of finite length structures using conventional SFEM based on Fourier transform requires the structures to be damped or use of throw off element to artificially induce damping. In addition, for such methods, the time window should be large to remove the wrap around problem. The time window is dependent on the damping and length, being more for lightly damped short length structures. WSFEM is completely free from such problems where the accuracy of solution is independent of these parameters. In Fig. 4 longitudinal velocities in the rod due to tip impact load are plotted considering $\eta = 0.5$. For the solution obtained using WSFE, the time window of $T_w = 512$ μs is sufficient, while for FSFEM time windows, T_w of 1024 μs, 2048 μs and 4096 μs and sampling time $\Delta t = 1$ μs are used. It can be seen that for $T_w = 1024$ μs (Fig. 4(a)) FSFE solution is highly distorted and the accuracy gradually increases with increase of T_w (Fig. 4(c)). Thus, the present spectral element results in substantial reduction of computational cost as the T_w is directly related to the system size.

In the numerical experiments presented the results obtained using periodic wavelets are not provided as they match exactly with the FSFEM solutions except the advantage of having multi-resolution analysis.

Next, numerical experiments are performed to study flexural wave propagation in an aluminum beam due to the unit impulse load (Fig. 2) applied at tip in transverse direction. The elastic properties and

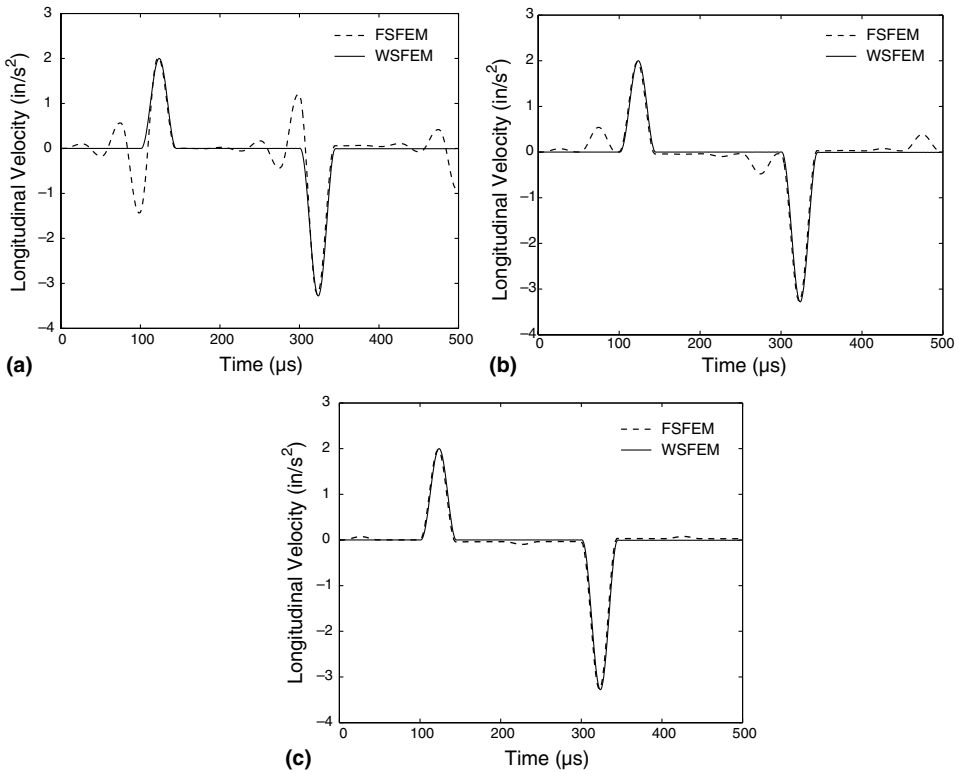

Fig. 4. Longitudinal tip velocity in rod due to tip impact load for time window T_w (a) $T_w = 1024$ μs (b) $T_w = 2048$ μs and (c) $T_w = 4096$ μs.

dimensions are same as the rod except that here the length L is even shorter and is equal to 10 in. The transverse velocity at the tip simulated using a single WSFE is shown in Fig. 5. A time window of $T_w = 2048$ μs with a sampling rate $\Delta t = 1$ μs, is used to solve the problem. It is also compared with FE result obtained using 400, 3 noded plane stress triangular elements. Figure shows excellent agreement between FE and WSFE solutions. As in the case of rod, FSFEM cannot be used for such undamped short length beam and the analysis requires consideration of damping or semi-infinite structures.

In Fig. 6, transverse velocity in the beam due to tip impact load is plotted considering a damping of $\eta = 0.5$. For the results obtained with wavelet spectral element, the time window used is $T_w = 1024$ μs, however as stated earlier the accuracy of the solution is independent of T_w. For conventional SFEM solutions, the time windows, T_w used are 1024 μs, 2048 μs and 4096 μs. It can be seen that the distortions gradually decrease by increasing T_w (Fig. 6(a)–(c)).

Finally wave propagation analysis is performed on a 2-D frame structure with a vertical load P applied as shown in Fig. 7. This example is much more complicated as multiple reflections occur from the joints and supports. For analysis of this structure, three spectral elements, for the three members are used and the elemental dynamic stiffness matrices of these members are assembled using standard FE technique.

In Fig. 8 the transverse wave velocity at point A (shown in Fig. 7) is presented and compared with FE result. The FE result is obtained using 2-noded 1-D beam element with an axial, transverse and rotational degree of freedom at each node. Each of the three members of the frame is discretized with 5000 elements. Results show very good agreement between these two solutions. Since FSFE cannot be used for similar analysis of undamped finite length structures, the wave velocities are plotted in Fig. 9(a)–(c) considering a damping of $\eta = 0.5$. In the above mentioned figures for all the plots obtained using wavelet, a time window T_w of 1024 μs is used. For FSFEM, T_w is increased from 1024 μs to 4096 μs in Fig. 9(a)–(c) to remove wrap around. It can be seen that for $T_w = 1024$ μs the results are highly distorted which gradually decreases with increase in T_w. In Fig. 9(c), even increasing T_w to 4096 μs is not capable of completely eliminating the response distortion. It further requires higher resolution.

The above numerical experiments have been done using basis function of order $N = 8$ and sampling rate $\Delta t = 1$ μs. Higher order basis functions approximate polynomials of increasingly higher orders and thus it is expected that for a given Δt, the solution will get refined further. Fig. 10(a) shows the refinement achieved using different basis functions for a given time window $T_w = 512$ μs. The tip longitudinal velocity shown in

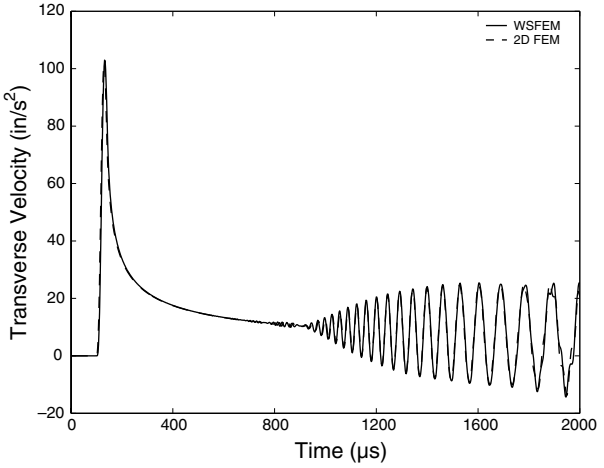

Fig. 5. Transverse tip velocity in beam due to tip impact load.

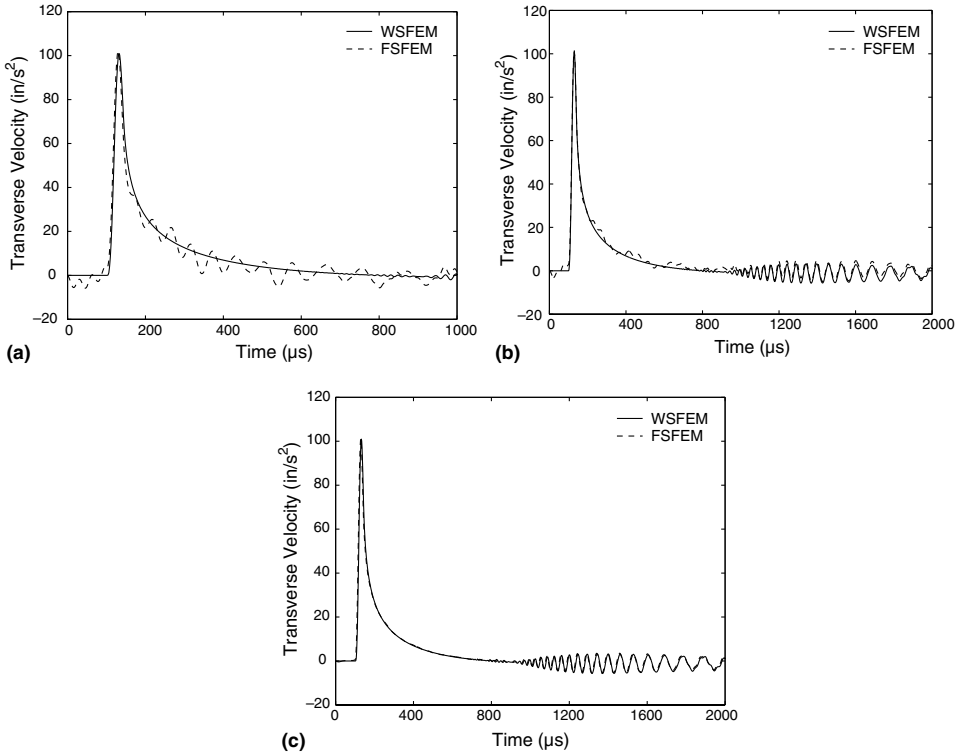

Fig. 6. Transverse tip velocity in beam due to tip impact load for time window T_w (a) $T_w = 1024$ μs (b) $T_w = 2048$ μs and (c) $T_w = 4096$ μs.

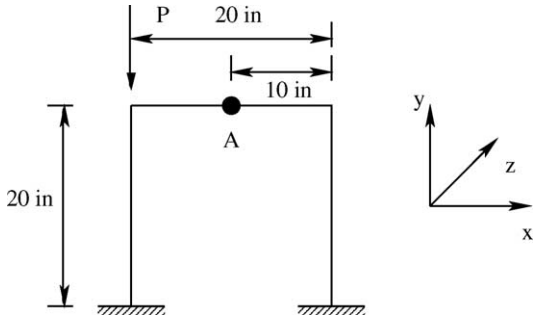

Fig. 7. 2-D frame structure.

Fig. 4 obtained using $N = 8$ and $\Delta t = 1$ μs is taken to be the most refined solution (v_f). The coarser solutions (v_c) are obtained by increasing Δt to 2 μs, 4 μs, 8 μs for a fixed T_w and thus decreasing the number of sampling points n. The error is obtained as $\|v_f - v_c\|/\sqrt{n}$ for different basis function and Δt. Fig. 10(a) shows that the error gradually decreases for $N = 6$ to $N = 20$. To show the dependence of T_w, the time window, for obtaining accurate solutions in FSFEM, the above error is plotted considering same v_f for fixed sampling rate of 2 μs. This is shown in Fig. 10(b). It is observed that the error gradually decreases with increasing T_w as distortion due to wrap around decreases. Also, for a particular T_w, the measured error does not vary much as the Δt is increased from 1 μs to 8 μs.

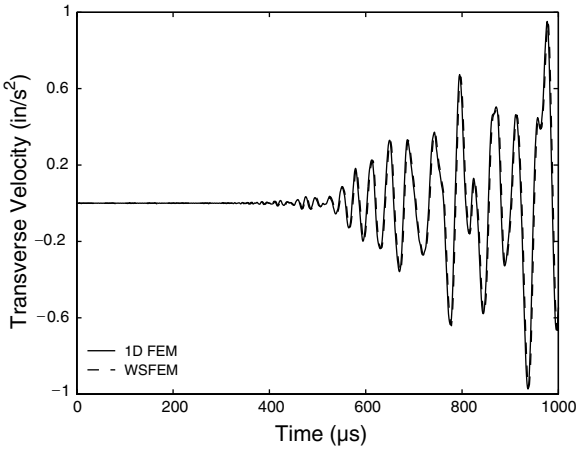

Fig. 8. Transverse velocity at A of 2-D frame in Fig. 7 due to the applied load P.

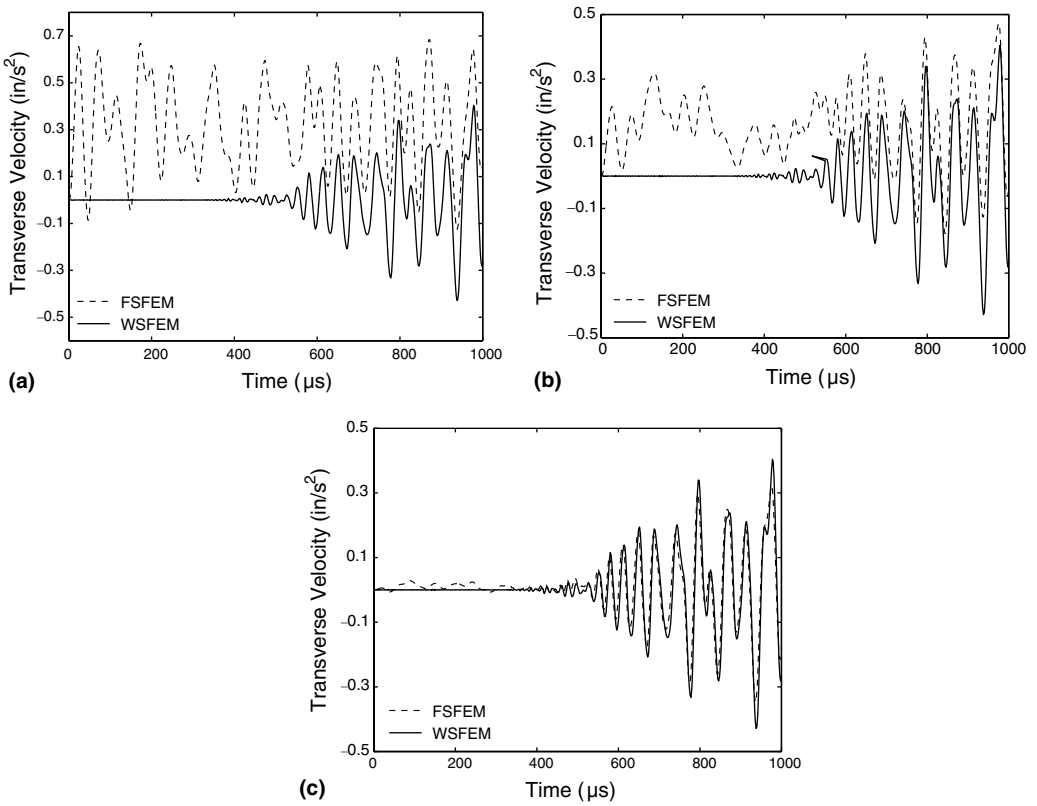

Fig. 9. Transverse tip velocity at A of 2-D frame in Fig. 7 due to the applied load P, for time windows T_w (a) $T_w = 1024$ μs (b) $T_w = 2048$ μs and (c) $T_w = 4096$ μs.

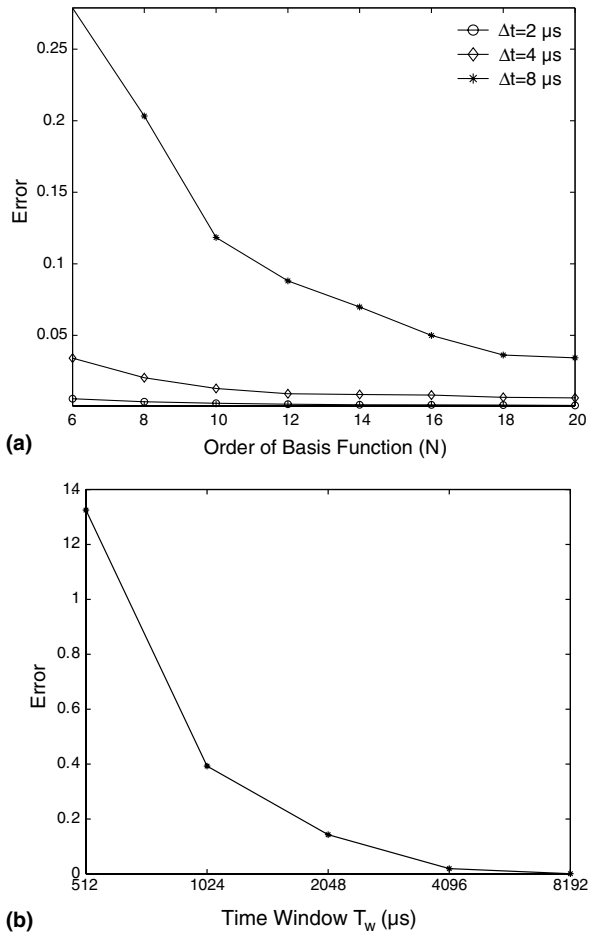

Fig. 10. Error as $\|v_f - v_c\|/\sqrt{n}$ for different (a) sampling rates Δt and order of basis (N) and (b) T_w using FSFEM.

6.2. Force identification

The earlier examples demonstrate the presence of wrap around problems in FSFE solutions. When such solutions are used to perform inverse problem such as force identification on a shorter waveguide, due to time window limitation, the solution obtained may yield a highly distorted force history. This is where the formulated WSFE will be of great utility. Its use in force identification is demonstrated in this section.

First, force identification from measured axial velocity is done considering undamped condition. The longitudinal velocity at the mid point of the rod due to tip axial load obtained using FE is used as input. The unit impulse load described in Section 6.1 and shown in Fig. 2 is used as the applied load to obtain the FE solution. The rod is modeled with 400, 3 noded plane stress triangular elements and the response is presented in Fig. 11. Fig. 12(a) shows the force reconstructed from the above response truncated at $T_c = 512$ μs, which shows excellent match with applied force. The forces identified from responses truncated at different points are same irrespective of the point of truncation (T_c). Thus this spectral element can efficiently reconstruct the force even from responses recorded for a small time duration. Similar to

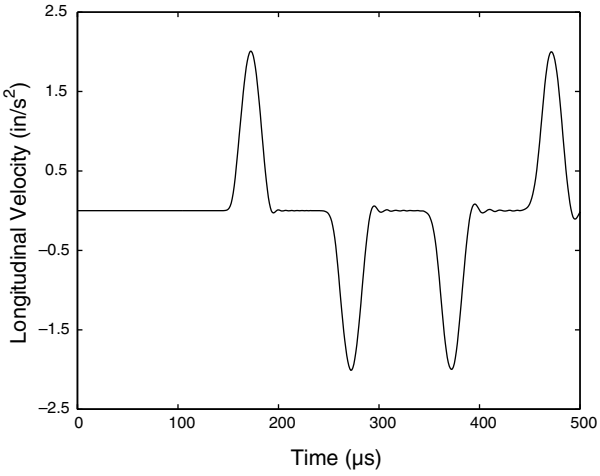

Fig. 11. Longitudinal velocity in rod measured at mid point ($x = 10$ in.) due axial impact load at tip ($x = 20$ in.) using 2-D FE.

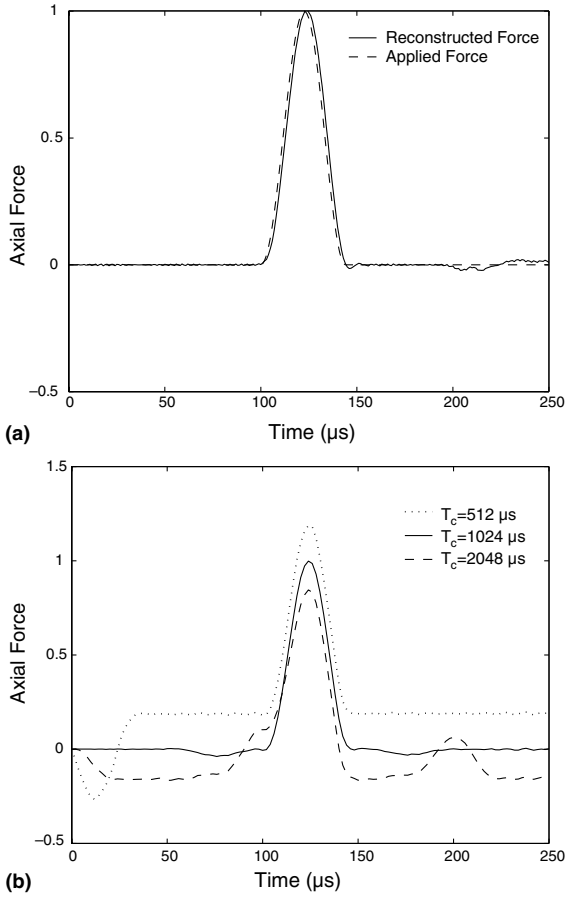

Fig. 12. Reconstructed impulse load applied to rod using (a) WSFEM and (b) FSFEM.

the forward problem in Section 6.1, FSFEM cannot be used for performing inverse problem in undamped finite length structure.

Though the above example shows the advantage of WSFE over FSFE in force identification, the reconstruction will involve certain problems when experimental data are used. This is because the experimental responses are never free from noise which causes distortion in the reconstructed force. In Fig. 13(a), a noisy response is simulated by adding white noise to the response shown in Fig. 11, to produce a signal to noise ratio of 7.5. The reconstructed force is shown in Fig. 13(b) and it can be seen that it is highly distorted. This example shows, that as mentioned earlier, when experimentally measured responses are used as input, denoising of the signal is required prior to reconstruction.

Next, we deal with damped structures to compare the results obtained using WSFEM and FSFEM. The response used as input is similar to that shown in Fig. 11 except that a damping of $\eta = 1.0$ is considered. The force reconstructed using wavelet in this case is very much similar to that presented in Fig. 12(a). Fig.

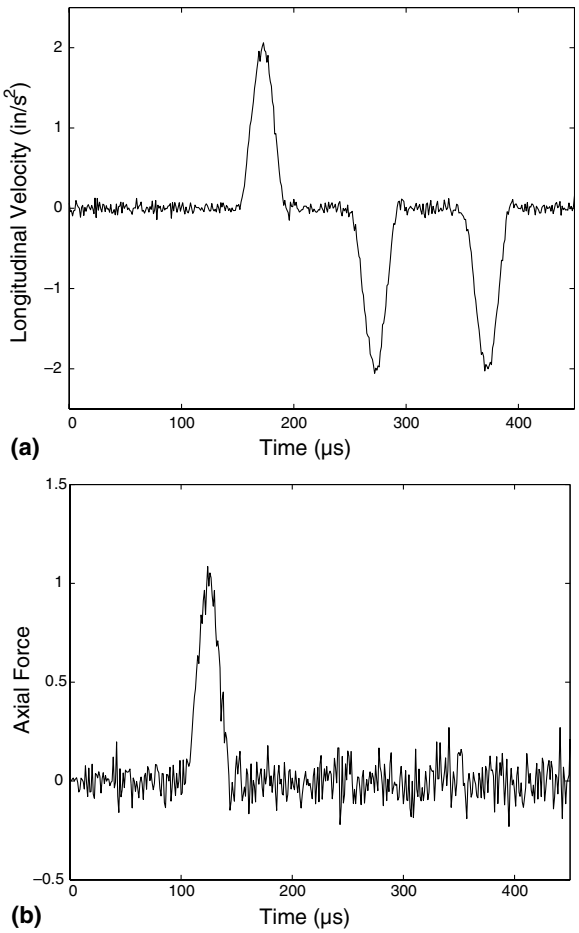

Fig. 13. Reconstruction of impulse load applied to rod (a) response used as input (Fig. 11 with simulated white noise) and (b) reconstructed impulse load.

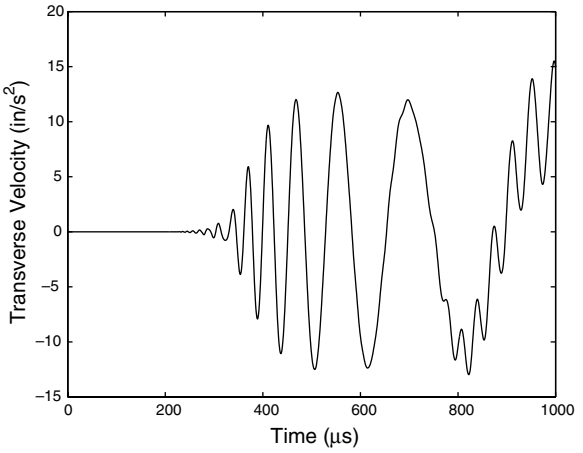

Fig. 14. Transverse velocity in beam measured at mid point ($x = 5$ in.) due transverse impact load at tip ($x = 10$ in.) using 2-D FEM.

12(b) presents the forces identified using FSFEM for different truncation points (T_c). It can be seen that for $T_c = 512$ μs, the force obtained is highly inaccurate and gradually gets refined with increased T_c.

Similar experiments are performed for force identification from recorded transverse velocity in beam. The flexural velocity measured at the mid point of the beam due tip impact load simulated using FE and shown in Fig. 14 is used as input. The impulse loading and the 2-D FE mesh used are same as that used for rod. First an undamped ($\eta = 0$) case is considered for which FSFEM is unable to predict the results. Fig. 15(a) shows the force reconstructed from the above response truncated at $T_c = 512$ μs using WSFE. As stated for the rod, force identification using WSFEM is independent of the point of truncation (T_c).

The response plotted in Fig. 14 with a damping of $\eta = 1.0$ is used as input next to compare the forces identified using WSFEM and FSFEM. The force reconstructed using wavelet has no interpretable difference from Fig. 15(a) and hence is not replotted. In Fig. 15(b) the force obtained using FSFEM is presented for $T_c = 512$ μs, 1024 μs and 2048 μs respectively. These plots reemphasize the advantages of WSFEM over FSFEM for inverse problems.

Finally force identification is done for the 2-D frame structure (Fig. 7) from the flexural response obtained through FE analysis and is shown in Fig. 8. The impulse loading is same as that used for rod and beam. The FE meshing is done with 5000 1-D beam element for each of the three members of the frame and a total of 15000 elements. Similar to the previous force identification experiments done, for 2-D frames WSFE reconstructs the impulse force accurately, irrespective of T_c and the plot is presented in Fig. 16(a). For this problem the forces identified using FSFEM and considering a damping of $\eta = 1.0$ are plotted in Fig. 16(b). It can be seen that for accurate reconstruction of force the method requires the truncation point $T_c = 4096$ μs which is higher than that required in previous examples of beam and rod. This can be justified as the response in this problem contains multiple reflections. Another way of using FSFEM for force identification from truncated responses, is to use throw-off element at the two fixed boundaries to release trapped energy. That is, the above 2-D frame (Fig. 7) can be thought of to be made of semi infinite members at the boundaries by adding throw-off element of stiffness 10 times that of the other members. The response simulated using FE, shown in Fig. 8 is used as input to the FSFE solver with throw-off element for force identification. The reconstructed forces are plotted in Fig. 16(c). The figure shows that for such complex structures, a large truncation point ($T_c = 4096$ μs) is required to get good results in FSFEM. However, these problems prove the efficiency of WSFEM in force reconstruction even for such complex structures.

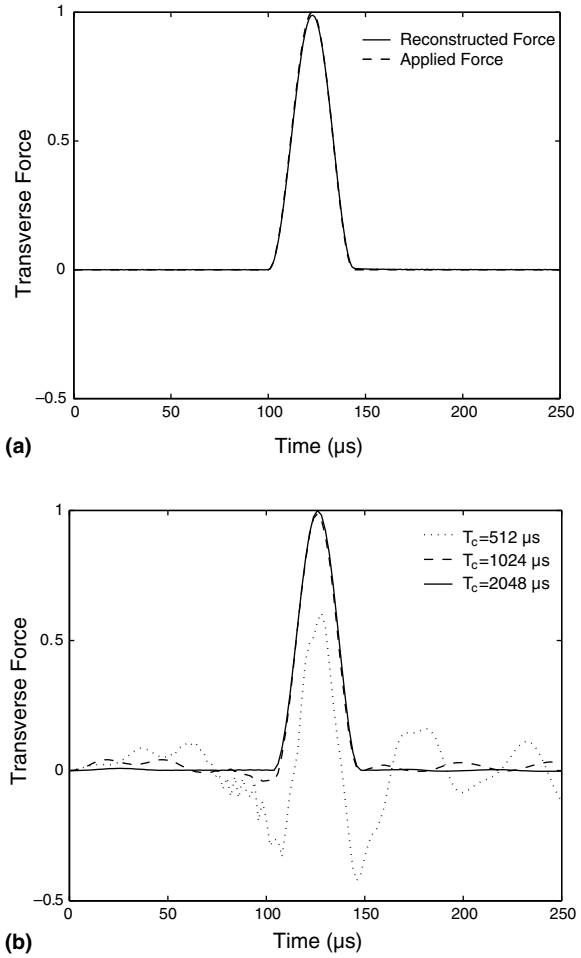

Fig. 15. Reconstructed impulse load applied to beam (a) WSFEM and (b) FSFEM.

7. Conclusions

This paper presents the formulation and validation of wavelet spectral element for simulation of wave propagation and force identification in rod, beam and 2-D frames. Spectral element method proves to be an efficient alternative of FE analysis of wave propagation problems and decreases the computational cost substantially. Moreover, SFEM can be used to perform inverse problems with great ease. The novelty of the spectral element developed is that it uses wavelet transform to reduce the PDEs to ODEs unlike the solution which is used in the SFE formulation. This wavelet based approach retains all the advantages of FSFEM, while it removes the problems associated with Fourier transform. First the axial and flexural velocities in undamped finite length structures obtained using present spectral element are validated with FE results. Next, numerical examples presented for damped finite length rod and beam show that wavelet spectral elements can remove the wrap around problem associated with the Fourier technique. This allows use of much smaller time window compared to FSFEM and thus decreases the cost substantially. The accuracy of identified force from the measured wave responses using FSFEM is determined by the point of truncation and the error is very high for small duration responses. The method proposed predicts the applied

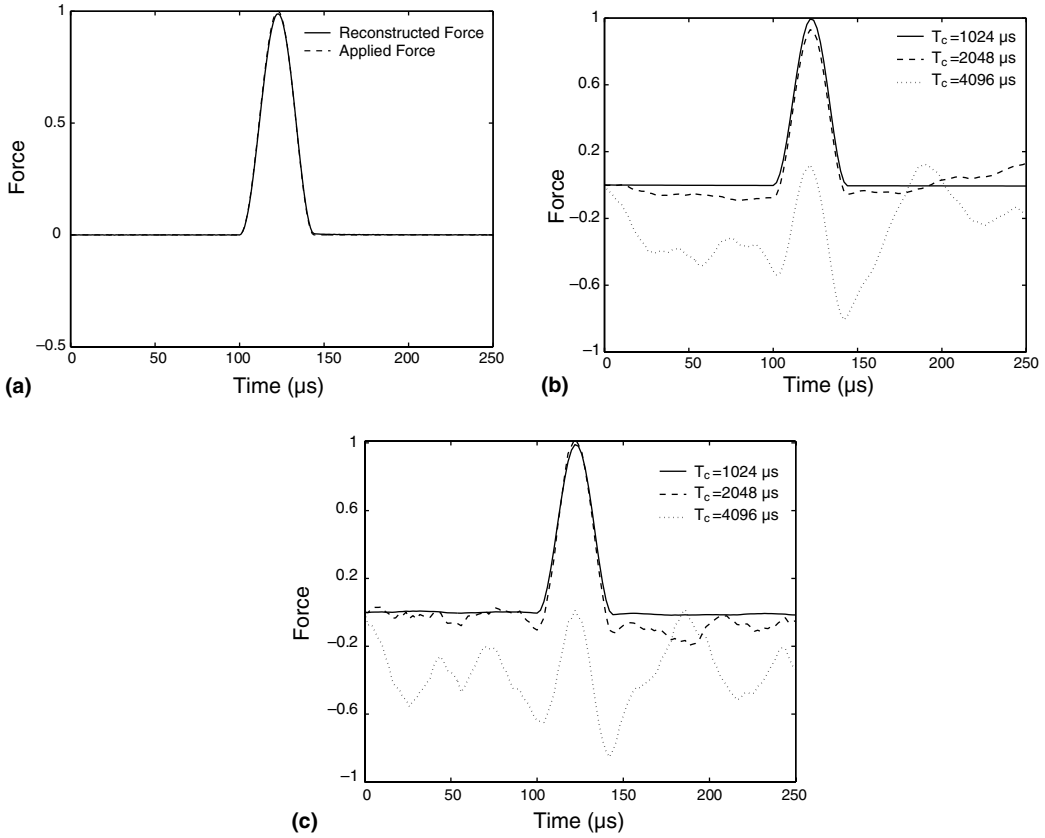

Fig. 16. Reconstructed impulse load applied to 2-D frame (a) WSFEM, (b) FSFEM and (c) FSFEM (with throw off).

force to a high degree of accuracy irrespective of truncation point, damping and length of structure. The reconstructed force may not be so accurate when experimentally measured responses are used as input, due to associated noise and complexities. Such cases will demand more refinement and/or modifications for efficient impulse load identification.

The scope of further research lies in the areas of extending the present formulation for 2-D PDEs. This may be done similarly to the FSFE formulation for semi-infinite plates presented by Chakraborty and Gopalakrishnan (in press). Alternatively, use of conventional FE for solutions of the transformed ODEs can be thought of instead of exact solution. The present WSFEM is restricted only to the analysis of linear elastic materials. Further work can be done to study the possibility of extending the present method for non-linear cases. A probable approach can be to update the WSFE solution of the non linear system after certain time step. The use of other compactly supported wavelet bases (B-spline wavelets) for spectral element formulation can also be studied.

References

Amaratunga, K., Williams, J.R., 1995. Time integration using wavelets. In: Proceedings of SPIE, Wavelet Application for Dual Use. 2491, Orlando, FL, pp. 894–902.

Amaratunga, K., Williams, J.R., 1997. Wavelet–Galerkin solution of boundary value problems. Archives of Computational Methods in Engineering 4 (3), 243–285.
Amaratunga, K., Williams, J.R., Qian, S., Weiss, J., 1993. Wavelet based Green's function approach to 2D PDEs'. Engineering Computation 10 (4), 349–367.
Amaratunga, K., Williams, J.R., Qian, S., Weiss, J., 1994. Wavelet–Galerkin solutions for one-dimensional partial differential equations. International Journal for Numerical Methods in Engineering 37, 2703–2716.
Beylkin, G., 1992. On the representation of operators in bases of compactly supported wavelets. SIAM Journal of Numerical Analysis 6 (6), 1716–1740.
Chakraborty, A., Gopalakrishnan, S., 2003a. A spectrally formulated finite element for wave propagation analysis in functionally graded beams. International Journal of Solids and Structures 40 (10), 2421–2448.
Chakraborty, A., Gopalakrishnan, S., 2003b. Force identification in a FGM plate using truncated response. 44th AIAA/ASME/ASCE/AHS-SDM Conference, Paper No. AIAA 2003-1590, Norfolk, Virginia.
Chakraborty, A., Gopalakrishnan, S., 2004. A spectrally formulated finite element for wave propagation analysis in layered composite media. International Journal of Solids and Structures 41 (18–19), 5155–5183.
Chakraborty, A., Gopalakrishnan, S., in press. A spectrally formulated plate element for wave propagation analysis in anisotropic material. Computer Methods in Applied Mechanics and Engineering.
Dahmen, W., 2001. Wavelet methods for PDEs some recent developments. Journal of Computational and Applied Mathematics 128 (1–2), 133–185.
Davis, P.J., 1963. Interpolation and Approximation. Blaisdell, New York.
Daubechis, I., 1988. Orthonormal bases of compactly supported wavelets. Communication in Pure and Applied Mathematics 41, 906–966.
Daubechis, I., 1992. Ten lectures on waveletsCBMS-NSF Series in Applied Mathematics. SIAM, Philadelphia.
Doyle, J.F., 1984. Further developments in determining the dynamic contact law. Experimental Mechanics 24, 265–270.
Doyle, J.F., 1987a. Determining the contact force during transverse impact of plates. Experimental Mechanics 27, 68–72.
Doyle, J.F., 1987b. Experimentally determining the contact force during the transverse impact of ortho-tropic plates. Journal of Sound and Vibration 118 (3), 441–448.
Doyle, J.F., 1988. A spectrally formulated finite element for longitudinal wave propagation. International Journal of Analytical and Experimental Modal Analysis 3, 1–5.
Doyle, J.F., Farris, T.N., 1990a. A spectrally formulated finite element for flexural wave propagation in beams. International Journal of Analytical and Experimental Modal Analysis 5, 13–23.
Doyle, J.F., Farris, T.N., 1990b. A spectrally formulated finite element for wave propagation in 3-D frame structures. International Journal of Analytical and Experimental Modal Analysis, 223–237.
Doyle, J.F., 1993. Force identification from dynamic response of a bi-material beam. Experimental Mechanics 33, 64–69.
Doyle, J.F., 1999. Wave Propagation in Structures. Springer, New York.
Doyle, J.F., 2002. Reconstructing dynamic events from time limited spatially distributed data. International Journal for Numerical Methods in Engineering 53, 2721–2734.
Elden, L., Berntsson, F., Reginska, T., 2000. Wavelet and Fourier methods for solving the sideways heat equation. SIAM Journal of Scientific Computing 21 (6), 2187–2205.
Glowinski, R., Lawton, W., Ravachol, M., Tanenbaum, E., 1990. Wavelet solution of linear and nonlinear elliptic, parabolic and hyperbolic problems in one space dimension. In: Proceedings of the 9th International Conference on Numerical Methods in Applied Sciences and Engineering, SIAM, Philadelphia.
Gopalakrishnan, S., Martin, F., Doyle, J.F., 1992. A matrix methodology for spectral analysis of wave propagation in multiple connected Timoshenko beam. Journal of Sound and Vibration 158, 11–24.
Hong, T.K., Kennett, B.L.N., 2002. On a wavelet based method for the numerical simulation of wave propagation. Journal of Computational Physics 183, 577–622.
Joly, P., Maday, Y., Perrier, V., 1994. Towards a method for solving partial differential equations by using wavelet packet bases. Computer Methods in Applied Mechanics and Engineering 116 (2), 193–202.
Joly, P., Komatitsch, D., Vilotte, J.P., 1995. The solution of the wave equation by wavelet basis approximation. In: Proceedings of the 1st Conference on Numerical Mathematics and Advanced Applications, Paris.
Latto, A., Resnikoff, H., Tanenbaum, E., 1991. The evaluation of connection coefficients of compactly supported wavelets. In: Proceedings of French-USA Workshop on Wavelets and Turbulence, Princeton University. Springer, New York.
Mahapatra, D.R., Gopalakrishnan, S., Shankar, T., 2000. Spectral-element-based solution for wave propagation analysis of multiply connected unsymmetric laminated composite beams. Journal of Sound and Vibrations 237 (5), 819–836.
Mahapatra, D.R., Gopalakrishnan, S., 2003. A spectral finite element model for analysis of axial flexural shear coupled wave propagation in laminated composite beams. Composite Structures 59 (1), 67–88.
Martin, F., Gopalakrishnan, S., Doyle, J.F., 1994. Wave propagation in multiply connected deep waveguides. Journal of Sound and Vibration 174 (4), 521–538.

Qian, S., Weiss, J., 1993a. Wavelets and the numerical solution of partial differential equations. Journal of Computational Physics 106 (1), 155–175.
Qian, S., Weiss, J., 1993b. Wavelets and the numerical solution of boundary value problems. Applied Mathematics Letter 6 (1), 47–52.
Reginska, T., 1995. Sideways heat equation and wavelets. Journal of Computational and Applied Mathematics 63, 209–214.
Reginska, T., Elden, L., 1997. Solving the sideways heat equation by a wavelet-Galerkin method. Inverse Problems 13, 1093–1106.
Rizzi, S.A., Doyle, J.F., 1991. Force identification for impact of a layered system. Computational Aspects of Contact, Impact and Penetration, Elmepress International, 222–241.
Robertsson, J.O.A., Blanch, J.O., Symes, W.W., Burrus, C.S., 1994. Galerkin–wavelet modeling of wave propagation: Optimal finite-difference stencil design. Mathematical Computations and Modelling 19, 31–38.
Vandergheynst, P., Antoine, J.-P., Van Vyve, E., Goldberg, A., Doghri, I., 2001. Modeling and simulation of an impact test using wavelets, analytical solutions and finite elements. International Journal of Solids and Structures 38, 5481–5508.
Williams, J.R., Amaratunga, K., 1994. Introduction to wavelets in engineering. International Journal for Numerical Methods in Engineering 37, 2365–2388.
Williams, J.R., Amaratunga, K., 1997. A Discrete wavelet transform without edge effects using wavelet extrapolation. Journal of Fourier Analysis and Applications 3 (4), 435–449.